Prediction of Frozen-In Birefringence in Oriented Glassy Polymers Using a Molecularly Aware Constitutive Model Allowing for Finite Molecular Extensibility

2 AUTHORS:

Davide S. A. De Focatiis
University of Nottingham
41 PUBLICATIONS **123** CITATIONS

SEE PROFILE

C. Paul Buckley
University of Oxford
119 PUBLICATIONS **1,456** CITATIONS

SEE PROFILE

Prediction of Frozen-In Birefringence in Oriented Glassy Polymers Using a Molecularly Aware Constitutive Model Allowing for Finite Molecular Extensibility

Davide S. A. De Focatiis*,† and C. Paul Buckley

Department of Engineering Science, University of Oxford, Oxford OX1 3PJ, U.K.

ABSTRACT: A study has been made of birefringence in oriented glassy polystyrene. The aim was to develop a methodology for the prediction of birefringence in glassy polymers with frozen-in molecular orientation. The predictive approach employed was to use a recently proposed constitutive model, consisting of a coupling between the Likhtman—Graham Rolie—Poly model for polymer melt rheology and a previously established model for polymer glasses. The methodology was validated with an experimental study of oriented glassy polystyrenes with known melt-stretching histories. It was found that, for orientation processes sufficiently far above T_g (i.e., not including subentanglement stretch), birefringence could be predicted accurately in monodisperse materials.
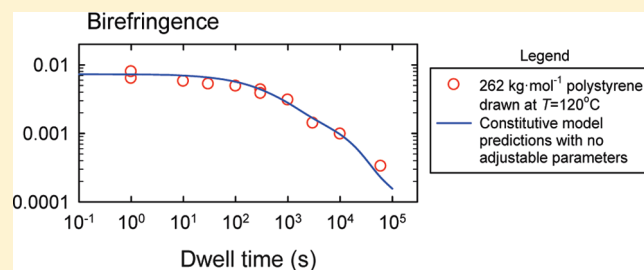
INTRODUCTION

Several optical properties of polymers exhibit anisotropy resulting from molecular orientation.[1] Frozen-in molecular orientation is an intrinsic feature of processed thermoplastic polymers in industrial products, unless special effort is made to allow the melt to relax prior to vitrification or crystallization. If specific optical properties are required in polymeric products, a quantitative understanding of the effects of process parameters such as deformation and temperature histories on these properties is required.

One of these optical properties, birefringence, or double refraction, is defined as the difference between the refractive indices for light plane-polarized parallel to two of the optic axes. Polarizability of individual monomers is anisotropic. It follows that any preferred alignment of them in a macroscopic sample of polymer results in macroscopic anisotropy of polarizability and hence anisotropy of refractive index and thus birefringence.[2] Since molecular alignment is a feature of the molecular conformations present, we shall refer to birefringence from this source as "conformational birefringence" Δn_c. This birefringence is of great practical interest, since it arises frequently during the shear and normal stresses typical of polymer processes such as extrusion and injection-molding at industrial rates. The rapid cooling usually employed in these processes then prevents molecular relaxation occurring subsequently and leaves the final solidified component with frozen-in molecular alignment and hence birefringence. This is important for two reasons. First, measuring the residual birefringence is a convenient means of determining experimentally the extent of residual molecular orientation in a polymer. Second, in some transparent polymer products the performance of the product itself relies on optical isotropy and hence the absence of birefringence.

Theoretical predictions of birefringence in processed amorphous polymers have been attempted by several authors, beginning with Tadmor's semiquantitative modeling.[3] Isayev and Hieber used a Leonov model to perform calculations of flow stress and birefringence in injection moldings[4] and later compared predictions to measurements on polystyrene (PS) and poly(methyl methacrylate) (PMMA) molded parts and runners.[5] This work was later extended by Flaman, who introduced a compressible Leonov model to account for packing pressure effects.[6,7] All of these studies employ viscoelastic constitutive equations parametrized to a greater or lesser extent by the rheological properties of the material to predict the resultant residual stresses in the material and, from these, the birefringence.

Recently, the present authors proposed a constitutive model for amorphous polymers able to cope seamlessly with both solid-state and melt-state deformations.[8] The model consists of a coupling of a previously proposed nonlinear viscoelastic model for polymer glasses, the Oxford glass—rubber model,[9] with the nonlinear rheological Rolie—Poly model,[10] derived as a simplification of a molecular theory.[11] The Oxford glass—rubber model was successfully applied to model large solid-state deformations in PS[12] and PMMA[13] and is formulated in such a way as to be easily implemented in finite element solvers. The Rolie—Poly model has been applied successfully within a Lagrangian flow solver[14] and validated on a wide range of complex flows.[15—17] The novel feature of the combined melt—solid constitutive model was the ability to *predict* the effects of molecular architecture (demonstrated by varying molar mass in monodisperse PS) on the resulting rheology and hence on the mechanical properties of glassy polymers with frozen-in orientation.[8]

The purpose of the present work was to investigate whether the combined melt—solid constitutive model could be applied to accurate

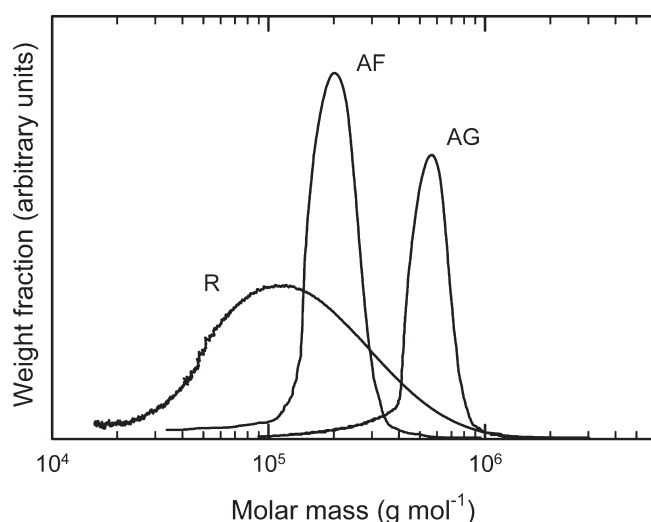**Table 1. Molar Mass Measurements Obtained by Triple Detection SEC for the Polystyrene Samples Used in This Study**

sample	MMD[a]	M_n (g mol^{-1})	M_w (g mol^{-1})	PDI[b]
AF	monodisperse	251 000	262 000	1.05
AG	monodisperse	449 000	518 000	1.15
R	polydisperse	85 900	218 000	2.54

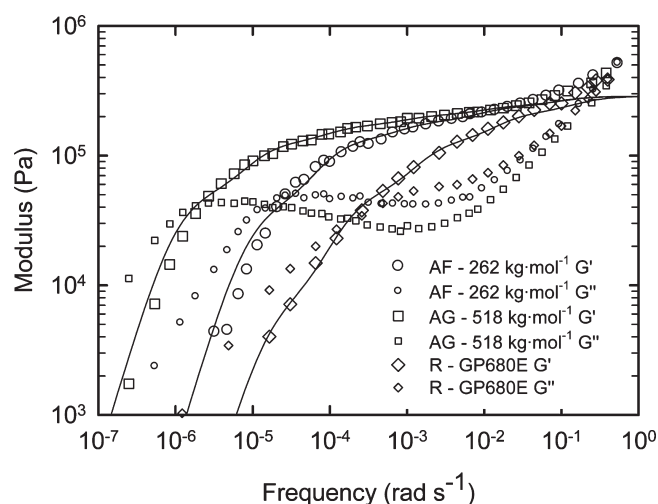[a] Molar mass distribution. [b] Polydispersity index.

Figure 1. Molar mass distributions of the three polymers studied in this work: AF and AG (monodisperse) and R (polydisperse) as obtained from size exclusion chromatography, kindly provided by Dr. Lian Hutchings.

Figure 2. Storage moduli (G', large symbols) and loss moduli (G'', small symbols) obtained from linear viscoelastic shear melt rheology for polymers AF, AG, and R, shifted to 120 °C using time−temperature superposition, for the three polymers used in this study. Also shown are the storage moduli computed from the discrete spectra of Maxwell modes used in the constitutive model (lines).

predictions of birefringence in oriented polymer products. A powerful feature of this approach is that the linear viscoelastic spectrum which parametrizes the Rolie−Poly part of the constitutive model can be predicted directly using the molecular theory of Likhtman and McLeish.[18] Therefore, prior rheological characterization for each molecular weight of interest is unnecessary in making predictions of orientation and birefringence of oriented polymer products.

■ EXPERIMENTAL SECTION

Materials and Characterization. The materials used in this study were samples of monodisperse and polydisperse linear atactic PS. Two monodisperse samples (M_w/M_n < 1.15) were synthesized by living anionic polymerization at Durham and were provided by Dr. Lian Hutchings of the University of Durham. One polydisperse sample (Dow GP680E base polymer with no additives) was provided by the Dow Chemical Company. Molar mass measurements were kindly performed by Dr. Hutchings by size exclusion chromatography (SEC) on a Viscotek TDA 302 machine with refractive index, viscosity, and light scattering detectors, and the results are given in Table 1. Measured molar mass distributions are shown in Figure 1. The codes used to refer to the polymers are consistent with previous publications on these polymers.[8,19,20]

Measurements of linear melt rheology in shear were kindly performed by Dr. John Embery of the University of Leeds, using 10 mm parallel plates on an Ares L2 rheometer. A temperature range of between 130 and 230 °C was used. The curves of G' and G'' versus log(frequency) were shifted using time−temperature superposition to provide a single

master curve for samples AF, AG ,and R at a reference temperature of 120 °C. The master curves are shown in Figure 2.

Sample Preparation. A steel mold with a central multicavity plate 0.5 mm in thickness sandwiched between upper and lower steel plates was used to mold rectangular bars in a hand-operated hydraulic press with heated platens. The steel cavity plate ensures accurate location of a series of removable steel inserts, which define the specimen geometry and allow for easy removal of the specimens after molding. Fresh sheets of disposable 0.15 mm thick soft temper 1200 aluminum foil, obtained from Multifoil Ltd., were used to line the top and bottom surfaces of the mold in order to provide a repeatable surface texture on the molded specimens. Prior to each molding operation, the inner surfaces of the mold, including the foil sheets, were lightly sprayed with a dry PTFE mold release aerosol. Each mold cavity was then filled with a small excess of polymer before placing the mold between preheated press platens. This molding technique was designed to cater for the limited availability of the monodisperse samples and kept material waste to a minimum by the near-net-shape production of rectangular bars, virtually eliminating the need for postmolding shaping.

The temperature during a typical molding cycle was monitored with an embedded thermocouple and can be found in our previous report.[19] The mold reached 170 °C in ∼10 min, during which time the platens were slowly closed. In order to dislodge any trapped air bubbles, the clamping force was cycled on and off manually for a period of 5 min. The mold was held at 170 °C at moderate pressure for a further 10 min to ensure relaxation and then cooled by flushing cold water through cooling channels in press platens, at a rate of ca. 15 °C min^{-1}. The mold was removed from the press when the temperature reached ∼70 °C. The moldings were verified as optically isotropic. Small amounts of flash were removed from the sides of the specimens after molding using fine grades of abrasive paper. Series of parallelepipedic bars with dimensions of 80 mm × 6 mm × 0.5 mm were produced using this technique.

Production of Oriented Specimens. The isotropic bars of PS were drawn uniaxially in an Instron 4204 testing machine fitted with an environmental chamber at a range of temperatures T near to and above T_g, at a constant crosshead velocity corresponding to a nominal strain rate of 0.02 s^{-1}. The bars were stretched to a range of draw ratios λ between 2 and 8, and then quench cooled to below T_g, using a cold spray applied at the end of the drawing process, giving an initial cooling rate of

$\sim 15\ ^{\circ}\text{C s}^{-1}$. In some experiments, after drawing and prior to quenching, a dwell time t_{dwell} was allowed for isothermal stress relaxation to occur at constant grip displacement. Temperature was monitored throughout the experiments using two thermocouples positioned close to the bars. The tensile load was recorded throughout the orientation process. Strain was monitored using a noncontact video extensometer. After freezing, the bars were wiped clean and stored in sealed bags at room temperature.

Optical Characterization of Oriented Specimens. The relative retardation r for the optic axes in the plane of the oriented bars was measured using an Olympus BX51 optical microscope fitted with polarizing optics and a thick Berek rotary compensator. Measurements were made by transmission through the full thickness of each bar at room temperature in white light. The optical birefringence Δn was then computed from $\Delta n = r/d$, where d is the specimen thickness measured by micrometer. Any residual thermal stress will be self-balancing and therefore will make no net contribution to the measured birefringence.

■ THEORY

Basis of a Constitutive Model Including Birefringence. The one-dimensional mechanical constitutive model of Haward and Thackray ascribed two contributions to the free energy and hence the stress.[21] The first arises from intermolecular and intramolecular bond stretching, and the second from perturbations of the conformational entropy of an entangled molecular network. The success of this approach in modeling the constitutive behavior of polymers is illustrated not only by the large number of citations,[22] more than 175 to date, but most importantly through the large number of constitutive models, including the one to follow, whose ideas build on those of Haward and Thackray.[9,12,23−29] But the physical origins of the two sources of stress are also the origins of the sources of birefringence in the glassy polymers of interest in this work.

In a phenyl polymer such as PS, optical birefringence has two distinct sources: (1) birefringence arising from bond stretching distortions through changes in interatomic distances, primarily in the carbon−carbon backbone, and (2) birefringence arising from molecular alignment through nonrandom molecular conformations and in the case of PS especially the phenyl side group.[30] In terms of the constitutive model employed in this work (see below) bond stretching is associated with a deviatoric stress state $\mathbf{S}_{\text{b}}$ and nonrandom molecular conformations are associated with a deviatoric stress state $\mathbf{S}_{\text{c}}$. For sufficiently small degrees of optical anisotropy, and assuming optic axes coincide with principal axes of stress, each contribution will obey a linear stress−optical rule relating the birefringence Δn to the corresponding differences in principal stress through a stress−optical coefficient C:

$$\Delta n_{\text{b}} = C_{\text{b}} \Delta S_{\text{b}}$$
$$\Delta n_{\text{c}} = C_{\text{c}} \Delta S_{\text{c}} \tag{1}$$

Here the subscript b stands for bond stretching, and c stands for conformational. In PS the two portions of birefringence have different signs. Typical values of the stress−optical coefficients reported for PS in the literature are $C_{\text{b}} = +8.3 \times 10^{-12}\ \text{Pa}^{-1}$ (measured at 27 °C)[31] and $C_{\text{c}} = -4.5 \times 10^{-9}\ \text{Pa}^{-1}$ (measured at 150 °C).[32] Since in PS the two parts of the birefringence are primarily attributed to different regions of the monomer, we follow previous authors in assuming that they are independent and additive,[33] and hence one may write

$$\Delta n = \Delta n_{\text{b}} + \Delta n_{\text{c}} \tag{2}$$

In fact, several authors have exploited this to show that the total birefringence changes sign during small strain stress-relaxation experiments, since the bond stretching stress relaxes faster than the conformational stress.[30,34]

On this basis we can extend the mechanical constitutive model to include birefringence in a glassy polymer such as PS. For example, when an isotropic PS is loaded to an infinitesimal strain state ε in the *glassy* state, parallel coupling means the bond stretching and conformational arms of the model are subject to identical strains. Therefore, the refractive index difference between any two optic axes is given by

$$\Delta n = \Delta n_{\text{b}} + \Delta n_{\text{c}} = C_{\text{b}} \Delta S_{\text{b}} + C_{\text{c}} \Delta S_{\text{c}}$$
$$= 2(C_{\text{b}} G_{\text{b}} + C_{\text{c}} G_{\text{c}}) \Delta \varepsilon \tag{3}$$

where G is a shear modulus and $\Delta \varepsilon$ is the corresponding difference in principal strains. The product of the stress−optical coefficient and modulus is approximately an order of magnitude larger for the bond stretching part than for the conformational part. This means that, since the stress−optical coefficients have different signs, the conformational part accounts for approximately a 10% reduction in birefringence when compared with bond stretching alone. Hence, for sufficiently small strains, the birefringence arising from bond distortion dominates in isotropic glassy PS.

When polymers are stretched in the *melt* and subsequently frozen and unloaded, they exhibit both forms of birefringence. This is because, in terms of the constitutive model, they are in a state of self-stress, with tensile conformational stresses being balanced by negative or compressive bond stretching stresses, or $\Delta S_{\text{b}} + \Delta S_{\text{c}} = 0$. Hence, the birefringence is given by

$$\Delta n = \Delta n_{\text{b}} + \Delta n_{\text{c}} = C_{\text{b}} \Delta S_{\text{b}} + C_{\text{c}} \Delta S_{\text{c}} = (C_{\text{c}} - C_{\text{b}}) \Delta S_{\text{c}} \tag{4}$$

It is noteworthy that, in the special case of PS, there is a considerable difference in magnitude between the stress−optical coefficients associated with the different sources of birefringence of the monomer ($C_{\text{c}}/C_{\text{b}} \approx -5500$). Therefore, the conformational birefringence associated with molecular orientation dominates, and $\Delta n \approx \Delta n_{\text{c}}$. In this case, the bond stretching birefringence accounts for less than 0.02% of the total. In polymers of different chemistry, this may not be the case, and both mechanisms may contribute significantly to the frozen-in birefringence.

Constitutive Model. The present authors recently proposed a new fully 3-dimensional model for the constitutive behavior of oriented PS,[8] based on a parallel coupling of a system of Rolie−Poly equations,[10] a previously published rheological model, and the bond stretching part of the Oxford glass−rubber constitutive model,[9] successfully used to model the solid-state response of PS below the glass transition.[12] The new melt−solid model was demonstrated to be qualitatively successful in capturing the effects of process-induced molecular orientation on the subsequent solid-state mechanical response under a wide range of orientation conditions. The model has been presented in detail previously,[8] and only a brief account will follow, highlighting the most important features and those which render this constitutive model *predictive* from a molecular perspective.

The constitutive model attributes the free energy of a deformed glassy polymer to two phenomena: local bond stretching perturbation of interatomic potentials and conformational changes of the entanglement network. The free energies, and hence the stresses, are assumed to be additive:

$$\mathbf{S} = \mathbf{S}_{\text{b}} + \mathbf{S}_{\text{c}} \tag{5}$$

where the tensor $\mathbf{S}$ refers to the deviatoric stress and the subscripts b and c refer to the bond stretching and conformational stresses, respectively. Under the conditions of this study, volumetric strains are small and are therefore modeled using linear elasticity as before.

Bond Stretching Part. The bond stretching stress is computed from a set of simultaneous differential governing equations that represent the evolution of stress in each bond stretching mode j. The deviatoric rate of deformation $\overline{\mathbf{D}}$ is related to the bond stretching deviatoric stress $\mathbf{S}_{\mathrm{b},j}$ and to the Jaumann rate of stress $\hat{\mathbf{S}}_{\mathrm{b},j}$ through

$$\overline{\mathbf{D}} = \frac{\hat{\mathbf{S}}_{\mathrm{b},j}}{2G_{\mathrm{b}}} + \frac{\mathbf{S}_{\mathrm{b},j}}{2G_{\mathrm{b}}\tau_j} \tag{6}$$

where G_{b} is the glassy shear modulus and τ_j is the relaxation time associated with mode j.

The total bond stretching stress can then be obtained as a weighted sum over all M modes

$$\mathbf{S}_{\mathrm{b}} = \sum_{j=1}^{M} v_j \mathbf{S}_{\mathrm{b},j} \tag{7}$$

Here v_j is refers to the volume fraction of material associated with relaxation time τ_j. The relaxation time of each mode is shifted relative to its value stress free, in structural equilibrium at a reference temperature, $\tau_{j,0}^*$, through a set of shift factors for temperature (a_{T}), structure (a_{S}), and stress ($a_{\sigma,j}$)

$$\tau_j = a_{\mathrm{T}} a_{\mathrm{S}} a_{\sigma,j} \tau_{j,0}^* \tag{8}$$

In this work we use the same material constants and shift factor equations as previously employed in a study on the same materials.[8] The reader is referred to previous publications for a justification of this approach.[8,9,12,23] For simplicity, we assume that deformations sufficiently above T_{g} take place in structural equilibrium (i.e., $a_{\mathrm{S}} = 1$).

Conformational Part. In order to account for the melt-state relaxations, we compute the conformational stress using the Rolie—Poly constitutive model.[10] The present work is concerned with large melt-state deformations and explores a wide time—temperature space including areas with limited relaxation. For this reason, the version of the Rolie—Poly model modified to account for finite molecular extensibility (FE) is used here.

For every conformational mode k, an orientation tensor $\mathbf{T}_k$ is defined, characterizing preferred orientation of end-to-end vectors between molecules *and* preferred orientation of molecular segments within molecules (i.e., molecular stretch) (see Appendix). The rms stretch of the kth mode is $\lambda_k = [^1/_3 \, \mathrm{tr}(\mathbf{T}_k)]^{1/2}$. From the Rolie—Poly model applied to the case of FE, and neglecting convective constraint release, $\mathbf{T}_k$ evolves with the deviatoric velocity gradient $\overline{\mathbf{L}}$ according to

$$\dot{\mathbf{T}}_k = \overline{\mathbf{L}} \cdot \mathbf{T}_k + \mathbf{T}_k \cdot \overline{\mathbf{L}}^{\mathrm{T}} - \frac{1}{\tau_{\mathrm{d},k}}(\mathbf{T}_k - \lambda_k^2 \mathbf{I}) - \frac{2}{\tau_{\mathrm{R},k}}\left(\frac{F(\lambda_k) - 1}{\lambda_k}\right)\mathbf{T}_k \tag{9}$$

where $\tau_{\mathrm{R},k}$ and $\tau_{\mathrm{d},k}$ are the Rouse and reptation times associated with the kth mode, and $F(\lambda_k)$ is given by

$$F(\lambda_k) = \frac{\lambda_{\max}}{3}\left[\frac{\lambda_{\max}^2 - 1}{\lambda_{\max}^2 - 1/3}\right]\mathscr{L}^{-1}\left(\frac{\lambda_k}{\lambda_{\max}}\right) \tag{10}$$
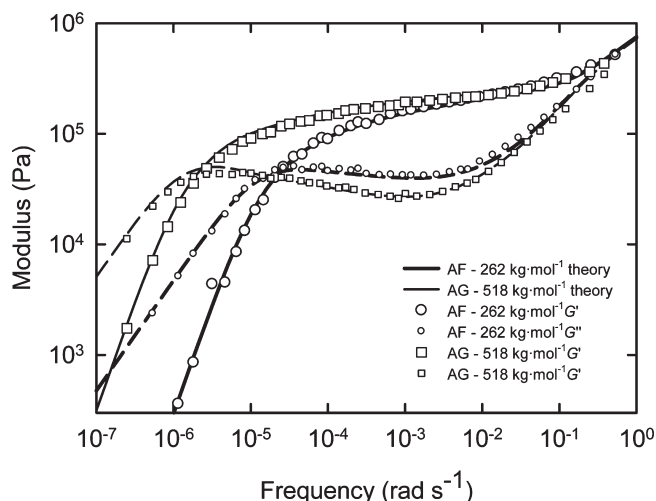

Figure 3. Storage moduli (G', large symbols) and loss moduli (G'', small symbols) for monodisperse polymers AF and AG obtained from linear viscoelastic shear melt rheology, shifted to 120 °C using time—temperature superposition. Also shown are the fits to the Likhtman—McLeish theory for AF and AG, using parameters G_{e} = 317.9 kPa, M_{e} = 13.14 kg/mol, and τ_{e} = 10.57 s at T^* = 120 °C (thick and medium lines, respectively; solid lines, G'; dashed lines, G'').

where $\mathscr{L}^{-1}$ indicates the inverse Langevin function and $\lambda_{\max}$ is the limiting stretch corresponding to full alignment of molecular segments. $F(\lambda)$ is defined in this way so that $F(\lambda) \to \lambda$ as $\lambda \to 1$. This is necessary in order to maintain consistency with the non-FE version of Rolie—Poly given by Likhtman and Graham.[10] See the Appendix for an explanation of the modification to account for FE.

The total conformational deviatoric stress is then computed from the weighted sum over all conformational modes

$$\mathbf{S}_{\mathrm{c}} = \sum_{k=1}^{N} v_k \frac{G_{\mathrm{e}}}{J}\left(\frac{F(\lambda_k)}{\lambda_k}\right)[\mathbf{T}_k - \lambda_k^2 \mathbf{I}] \tag{11}$$

where v_k is the weighting of mode k, G_{e} is the entanglement modulus, and J is the volume ratio(see the Appendix for explanation).

The Rouse and reptation times are shifted relative to a reference temperature and structure through shift factors ($\tau_{\mathrm{R},j} = a_{\mathrm{T}} a_{\mathrm{S}} \tau_{\mathrm{R},j}^*$ and $\tau_{\mathrm{d},j} = a_{\mathrm{T}} a_{\mathrm{S}} \tau_{\mathrm{d},j}^*$) as defined in our earlier publication.[8]

Constitutive Model Parameters. Conformational model parameters G_{e}, M_{e} (the molar mass of one entanglement length), and τ_{e} (the Rouse time of one entanglement length) were obtained by using the microscopic theory of linear polymer melts of Likhtman and McLeish[18] applied to linear rheological data in shear simultaneously for the two monodisperse materials through the optimizer Reptate.[35]

The values used are as obtained in our previous publication:[8] G_{e} = 317.9 kPa, M_{e} = 13.14 kg mol^{-1}, and τ_{e} = 10.57 s at the reference temperature T^* = 120 °C. Following Collis et al.,[17] we then calculate the longest Rouse and reptation times from

$$\tau_{\mathrm{R},1}^* = Z^2 \tau_{\mathrm{e}}$$
$$\tau_{\mathrm{d},1}^* = 3\left(1 - \frac{2.38}{Z^{0.5}} + \frac{4.17}{Z} - \frac{1.55}{Z^{1.5}}\right)Z^3 \tau_{\mathrm{e}} \tag{12}$$

where $Z = M/M_{\mathrm{e}}$ is the number of entanglements per molecule. This connection to molecular theory is what allows genuine

predictive capability. Once a material such as PS is characterized through the parameters G_e, M_e, and τ_e, the linear viscoelastic spectrum for other grades of PS can be accurately predicted by the theory. It must be pointed out, however, that this capability is at present only possible for monodisperse materials.

The calculated linear viscoelastic responses, after fitting parameters G_e, M_e, and τ_e to the experimental data for materials AF and AG, are shown in Figure 3. They are compared to the experimentally recorded rheological measurements in order to illustrate the quality of the fit.

The parameter λ_{max} that defines the finite extensibility (FE) of chains in eq 10 is derived from molecular theory using an equivalent Kuhn chain between entanglements and is given by[8]

$$\lambda_{max} = \sqrt{\frac{n_b}{C_\infty}}\sin(\theta_b/2) \quad (13)$$

where n_b is the number of bonds between entanglements, C_∞ is the characteristic ratio for PS, and θ_b is the carbon–carbon backbone bond angle. Applying values of $C_\infty = 10$ and $\theta_b = 109.28°$ previously used for PS[8,12] and n_b obtained from M_e gives $\lambda_{max} = 4.09$.

Both the glassy and the conformational parts of the model approximate the physical relaxation spectrum by an empirical discrete spectrum. The spectrum was obtained by starting with the mode with the longest relaxation time, $\tau_{d,1}$, and attributing one mode per decade of time/frequency to cover the range of data of interest. The longest modes are conformational, until $\sum_{k=1}^{N}G_k = G_e$, and the remaining modes are glassy. A custom-built optimizer was written in Matlab to minimize the rms error between the computed and experimental values of $\log(G')$ and $\log(G'')$. The reader is referred to our previous publication for a detailed and illustrated account of this process.[8] For the purpose of calculations of relaxation times, we use $Z = M_w/M_e$. All other constitutive model parameters used in this study are taken from the earlier paper.[8]

A numerical implementation of the model has been coded in Matlab. Figure 2 illustrates the computed values of $\log G'$ for all three materials. Simulations were performed with the computed spectra for each material and test condition and included the melt-drawing phase, any dwell time, the quenching, and the unloading to zero stress.

Calculation of Birefringence. In the case of small orientations, where the distribution of the end-to-end vectors of the chain segments is Gaussian, the conformational birefringence can be computed from a constitutive model for a given stress state by straightforward use of the stress–optical rule. This is because, for Gaussian chains, both the stress and birefringence are proportional to the same measure of average segmental orientation,[36] or in terms of the present model both Δn and ΔS_c are proportional to ΔT. For example, for uniaxial extension in the 3 direction, birefringence in the 1–3 plane is given by

$$\Delta n_c = (n_{c,3} - n_{c,1}) = C_c\Delta S_c = C_c(S_{c,3} - S_{c,1}) \quad (14)$$

where $S_{c,i}$ is the ith principal component of the conformational deviatoric stress tensor $\mathbf{S}_c$.

The present constitutive model is designed, however, to deal with large orientations and stretches and incorporates finite chain extensibility. In this case, a nonlinear relationship exists between force and end-to-end distance in chains at large extensions. The resulting well-known effect is that birefringence saturates while conformational stress continues to grow, as previously shown experimentally by a number of authors.[37,38]

Consider a freely orienting molecule with end-to-end vector $\mathbf{R}$ represented by a chain of n transversely anisotropic units of length l, each with polarizability anisotropy $\Delta\alpha^{unit} = \alpha_\parallel^{unit} - \alpha_\perp^{unit}$. Kuhn and Grun derived the anisotropy of the whole chain allowing for finite extensibility,[39,40] expressed with respect to axes parallel and perpendicular to $\mathbf{R}$, as follows:

$$\Delta\alpha^{chain} = n\Delta\alpha^{unit}\left[1 - \frac{\frac{3R}{nl}}{\mathscr{L}^{-1}\left(\frac{R}{nl}\right)}\right] \quad (15)$$

In terms of this, the polarizability tensor of the chain may be written as

$$\boldsymbol{\alpha}^{chain} = \alpha_\perp^{chain}\mathbf{I} + \Delta\alpha^{chain}\frac{\mathbf{R}\mathbf{R}^T}{R^2} \quad (16)$$

Combining eqs 15 and 16, and approximating the average chain polarizability as that of a chain with the ensemble rms average R (indicated by brackets $\langle...\rangle$), allows calculation of the polarizability tensor per unit volume

$$\boldsymbol{\alpha} = \frac{N}{J}\left\{\alpha_\perp^{chain}\mathbf{I} + \langle\Delta\alpha^{chain}\rangle\frac{\langle R_0^2\rangle}{\langle R^2\rangle}\frac{\langle\mathbf{R}\mathbf{R}^T\rangle}{\langle R_0^2\rangle}\right\} \quad (17)$$

where N is the number density of chains. Equation 17 may be rewritten in terms of $\mathbf{T}$ and λ as follows

$$\boldsymbol{\alpha} = \frac{N}{J}\left\{\alpha_\perp^{chain}\mathbf{I} + \frac{n(\alpha_\parallel^{unit} - \alpha_\perp^{unit})}{3\lambda^2}\left[1 - \frac{3(\lambda/\lambda_{max})}{\mathscr{L}^{-1}(\lambda/\lambda_{max})}\right]\mathbf{T}\right\} \quad (18)$$

and hence the polarizability anisotropy (difference between two eigenvalues) is

$$\Delta\alpha = \frac{N}{J}\frac{(\alpha_\parallel^{unit} - \alpha_\perp^{unit})}{3}\left(\frac{\lambda_{max}}{\lambda}\right)^2\left[1 - \frac{3(\lambda/\lambda_{max})}{\mathscr{L}^{-1}(\lambda/\lambda_{max})}\right]\Delta T \quad (19)$$

A similar conclusion was reached previously by Arruda and Przybylo for elastomers, using the "8-chain" model.[41]

It is convenient to express eq 19 in the form

$$\Delta\alpha = \frac{N}{J}\frac{(\alpha_\parallel^{unit} - \alpha_\perp^{unit})}{5}H\left(\frac{\lambda}{\lambda_{max}}\right)\Delta T,$$

$$\text{where } H(x) \equiv \frac{5}{3x^2}\left[1 - \frac{3x}{\mathscr{L}^{-1}(x)}\right] \quad (20)$$

In the limit $\lambda \to 1$ there is a linear photoelastic response and linear elastic response (see eqs 1 and the linear limit of eq 11)

$$\Delta n_c = C_c\Delta S_c; \quad \Delta S_c = G_e\Delta T \quad (21)$$

Given the physical proportionality between Δn_c and $\Delta\alpha$, it follows that the birefringence can be calculated from $\mathbf{T}$ for arbitrary λ as follows:

$$\Delta n_c = C_c G_e\frac{H\left(\frac{\lambda}{\lambda_{max}}\right)}{H\left(\frac{1}{\lambda_{max}}\right)}\Delta T \quad (22)$$
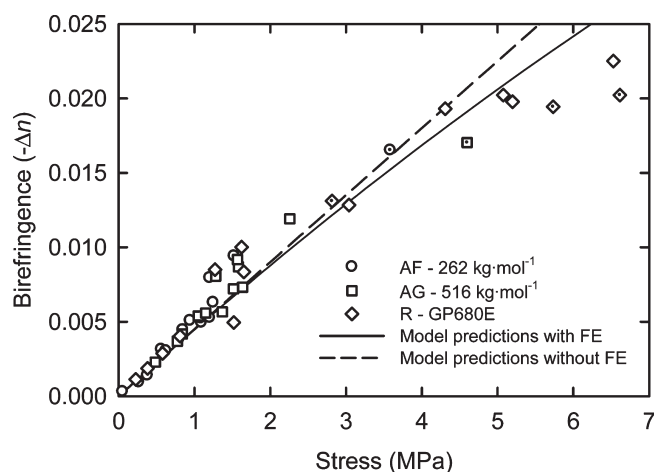
Figure 4. Measurements of birefringence plotted versus the stress immediately prior to quenching for materials AF, AG, and R (symbols). Experiments performed at $T \leq 110\ °C$, where a yield stress was measurable, are marked with a dot. Simulation predictions of the birefringence−stress relation, assuming a stress−optical coefficient $C_c = -4.5 \times 10^{-9}\ Pa^{-1}$, with FE (solid line) and without FE (dashed line).

For the multimodal approach used in this work, and for the simple case of uniaxial deformation in the 3 direction, birefringence may therefore be obtained from

$$\Delta n_c = C_c G_e \sum_{k=1}^{N} \nu_k (T_{k,3} - T_{k,1}) \frac{H\left(\frac{\lambda_k}{\lambda_{max}}\right)}{H\left(\frac{1}{\lambda_{max}}\right)} \qquad (23)$$

where $T_{j,1}$ and $T_{j,3}$ are the eigenvalues of the jth orientation tensor associated with directions 1 and 3. In this work the multiplier $H(x)$ was evaluated using the highly accurate Treloar[42] three-term approximation of the square bracket in eq 20, giving

$$H(x) \simeq 1 + \frac{x^2}{3} + \frac{x^4}{3} \qquad (24)$$

If necessary, the bond stretching contribution to birefringence can also be computed by the use of the stress−optical rule on the bond stretching stress from the constitutive model, although the effect of time and temperature on the distortional stress−optical coefficient may need to be included. For the specific case of oriented PS illustrated in the present paper, however, this contribution was neglected for the reason given earlier.

In the simulations of birefringence that follow, a standard literature value of $C_c = -4.5 \times 10^{-9}\ Pa^{-1}$ (measured at $150\ °C$)[32] was used throughout. Birefringence was computed from the orientation tensor remaining at the end of the simulation process, after the deformation, any dwell time, a rapid quench, and an unloading resulting in specimens in a state of self-stress under no applied loads.

■ RESULTS AND DISCUSSION

Stress−Birefringence Relationship. Equation 11 shows that, to a good approximation, the conformational stress depends only on orientation **T** (neglecting the secondary effects of varying absolute temperature T and dilation J). Also, eq 22 shows that birefringence depends only on **T** to the same approximation.

Therefore, we predict a unique relationship exists between conformational stress and birefringence, even extending to large degrees of orientation where the effect of FE is significant.

This is tested in Figure 4, showing all the measurements of room temperature birefringence for the present set of oriented specimens, prepared as described above (45 data points in total). The birefringence is plotted versus the true stress recorded immediately prior to the quench for drawn specimens of materials AF, AG, and R, oriented using a wide range of conditions. For drawing at $T \leq 110\ °C$ a measurable yield stress was recorded (indicating a residual contribution from the b-stress): these data are marked with a dot. For small stresses prior to the quench there is a linear relationship between stress and birefringence, and the classical stress−optical rule that assumes Gaussian chains applies, even though the birefringence was measured on glassy samples at room temperature. However, when the stress in the melt becomes larger than ∼4 MPa, a deviation from linearity is observed. The nonlinearity can be partly explained by a residual contribution from the b-stress for some of the experimental data; this effect is also clearly visible, for instance, in the simultaneous stress−birefringence measurements during stretching performed by Muller and Pesce.[37] However, even in the more limited data set for which no yield stress was observed, the stress rises faster than the birefringence. This is a consequence of finite chain extensibility, and the tendency of birefringence to saturate at high degrees of stretch, while the stress continues to rise. Our measurements of frozen-in birefringence in solid samples are consistent with the in-situ findings of Muller and Pesce, who also found that the *linear* stress−optical rule is obeyed only at high temperatures where the stress is relatively low. We suggest that deviations from linearity in which a *greater* birefringence is measured than that which is indicated by the stress−optical rule can either be due to inhomogeneities within the sample or from subentanglement stretch, as will be discussed later in the text.

Figure 4 also shows simulations of conformational stress and birefringence, computed with two versions of the constitutive model: the full model including FE and a simplified version neglecting FE (i.e., employing the approximations $F(\lambda_k) = \lambda_k$ and $H(\lambda_k/\lambda_{max})/H(1/\lambda_{max}) = 1$). The predictions of the two models are indistinguishable only for the smallest stresses.

It was previously suggested that the validity of a linear stress−optical rule to within experimental uncertainty is limited to stresses up to ∼2 MPa for PS.[43] In our simulations the computed difference between the model with FE and the model without FE reaches 1% at ∼1.1 MPa using the value of $\lambda_{max} = 4.09$. Although the scatter in the experimental data precludes a more precise evaluation of the deviation from linearity of the stress−optical rule, it is nevertheless clear that the model with FE is more consistent with the range of experimental data obtained in this paper than the model without FE.

The Role of Draw Temperature. In the results that follow, it will be useful to characterize the drawing regime by the use of Weissenberg numbers associated with various relaxation times of the polymer. For example, $Wi_d^{AF} = \tau_d^{AF} \dot{\varepsilon}$ is the Weissenberg number associated with the disengagement or reptation time τ_d^{AF} of polymer AF for a strain rate $\dot{\varepsilon}$. As the samples were drawn at constant crosshead extension rate corresponding to a nominal strain rate $\dot{\varepsilon}_{nom}$, the true strain rate $\dot{\varepsilon}_{true}$ is changing during stretching and is given by $\dot{\varepsilon}_{true} = \dot{\varepsilon}_{nom}/\lambda$. In the calculation of Weissenberg numbers referred to here, the nominal strain rate (equal to the true strain rate only at the beginning of each experiment) is used. Weissenberg numbers associated with the longest Rouse time (Wi_R^{AF}) and with
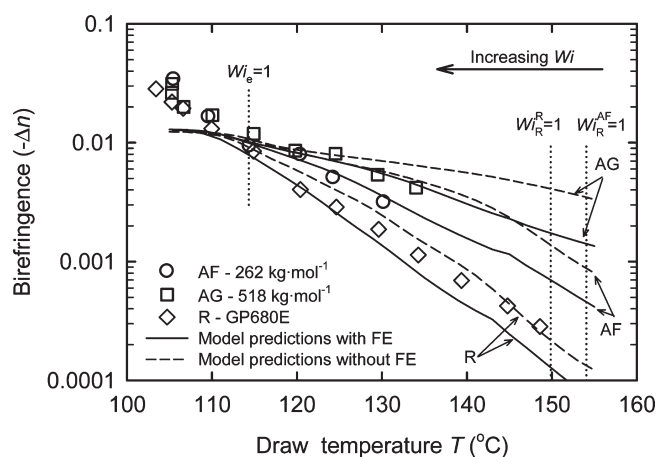
Figure 5. Measurements of birefringence as a function of hot-drawing temperature for materials AF, AG, and R (symbols). Drawing was performed at a strain rate of 0.02 s^{-1}, to a draw ratio $\lambda = 3$, and specimens were immediately quenched after drawing. Simulation predictions of birefringence computed using models with (solid lines) and without (dashed lines) finite extensibility. Also illustrated are the temperatures at which the τ_e- and τ_R-based Weissenberg numbers are equal to unity. $Wi_R^{AG} = 1$ occurs at 174 °C (not shown).

the Rouse time of one entanglement length (Wi_e) are defined similarly in terms of the corresponding relaxation times τ_R^{AF} and τ_e. A Weissenberg number greater than unity implies that relaxation does not occur during stretching on the length scale associated with the corresponding relaxation time.

Figure 5 shows measurements of birefringence made on the oriented bars as a function of drawing temperature T for materials AF, AG, and R, following hot drawing at a range of temperatures from 105 to 135 °C and immediate quenching using the cold spray. At lower drawing temperatures, particularly in the range where $Wi_e > 1$ ($T < 114$ °C under these conditions), there is little difference in birefringence beyond the experimental scatter across the three materials. At higher drawing temperatures, the material of highest molar mass displays the largest birefringence, indicating the largest orientation. It was not possible to draw the monodisperse materials AF and AG at higher temperatures than those displayed in Figure 5 as they were prone to tearing near the grips during stretching.

Also shown in Figure 5 are simulations of birefringence computed from the constitutive model. Simulations from the version of the constitutive model that incorporates FE are shown as solid lines; simulations from the simplified version without FE are shown as dashed lines. There are three important observations that can be made when comparing experimental results to simulations.

(1) For monodisperse materials AF and AG, the constitutive model (solid lines, with FE) accurately predicts birefringence for a wide range of hot-drawing temperatures for $Wi_e < 1$ but underpredicts the birefringence for $Wi_e > 1$.

(2) For the polydisperse material R, the constitutive model (solid line, with FE) accurately predicts the birefringence only for a narrow range of hot drawing at $Wi_e < 1$. The model underpredicts the birefringence for $Wi_e > 1$ and also underpredicts the birefringence for the higher draw temperatures, $Wi_e < 1$.

(3) For accurate predictions of birefringence in monodisperse materials under the conditions of this study, finite chain extensibility is an essential part of the model. In all cases

the removal of FE leads to an overprediction of birefringence for $Wi_e < 1$, as can be seen by the dashed lines.

In response to the first observation, the reader is reminded that the constitutive model consists of a series of conformational modes whose intrinsic physics takes into account effects of orientation of the entanglement network and a series of bond stretching modes which describe *isotropic* viscoplastic flow. When $Wi_e > 1$, stretching is taking place on a subentanglement length scale, and presently there is no means of accounting for this within the constitutive model. The authors found similar difficulties in accurately capturing the *glassy* constitutive response of oriented PS when the orientation had been performed at $Wi_e > 1$.[8] One possible route to the determination of what constitutes a length scale that is long enough to feel conformational changes may be to use experimental evidence of conformational birefringence. However, this is likely to be a difficult task, since the phenyl side group which contributes to conformational birefringence may not maintain the same angle to the main chain when deformed too close to T_g. The angle of the phenyl group of poly(styrene-*co*-acrylonitrile) was been observed to rotate when deformed in the glassy state.[44]

The second observation concerns the lack of fit for the polydisperse material R. Again, it should be pointed out that the Rolie−Poly equation was developed from a molecular theory for *monodisperse* melts. In the work presented here, for polymer R we have explored the use of this model in its present form for a polydisperse material, by computing the relaxation times associated with an equivalent monodisperse material with $M = M_w$, with modes fitted to the actual measured linear viscoelastic spectrum. This leads to an overprediction of the short relaxation times and an underprediction of the long relaxation times. At higher temperatures, the long relaxation times dominate, and hence the model overpredicts stresses and consequently birefringence. From a modeling perspective, a polydisperse material differs from a monodisperse material principally through the additional constraint release provided by the relaxation of the short chains. At present, this is unaccounted for in the constitutive model.

The third observation concerns the need for finite chain extensibility. Finite extensibility in this context has two effects. The first, which can be seen clearly in Figure 4, is to induce a saturation of birefringence at large orientations and stresses. This effect originates primarily through the inverse Langevin term in eq 15. The second, visible in Figure 5, is to enhance chain retraction at large stretches. This effect, originating from the inverse Langevin term in eq 10, leads to an earlier onset of the saturation of the stretch of the chains than would be present without finite chain extensibility. It is clear from the evidence presented that finite chain extensibility is necessary to enable accurate predictions of birefringence for the test conditions illustrated.

The Role of Dwell Time. The dwell regime may be characterized by the use of Deborah numbers associated with relaxation times of the polymer. For example, $De_d^{AF} = \tau_d^{AF}/t_{dwell}$ is the Deborah number associated with the reptation time of polymer AF. Deborah numbers associated with the longest Rouse time (De_R^{AF}) and with the Rouse time of one entanglement length (De_e) are defined similarly. A Deborah number greater than unity implies that relaxation does not take place during the dwell time on the associated length scale.

Figure 6a illustrates measurements of optical birefringence as a function of dwell time t_{dwell} after stretching and prior to freezing, for material AF drawn to $\lambda = 3$ at 120 °C and relaxed for t_{dwell}

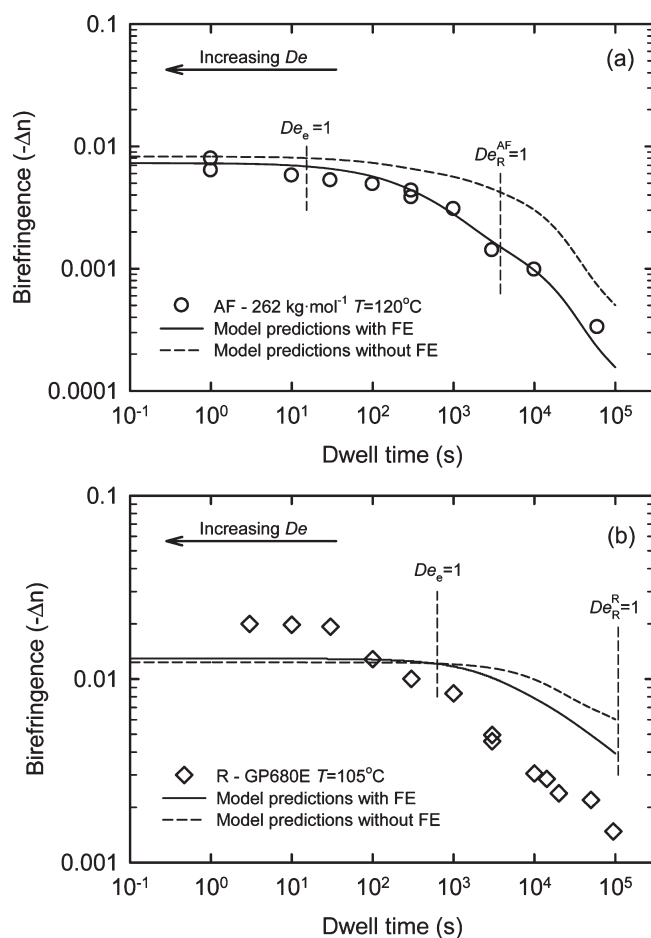**Figure 7.** Measurements of birefringence as a function of draw ratio for materials AG and R. Drawing was performed at a strain rate of 0.02 s^{-1}, at a temperature of 135 °C, to varying draw ratios, and was followed by immediate quenching. Simulation predictions of birefringence computed using models with (solid lines) and without (dashed lines) finite extensibility.

Figure 6. Measurements of birefringence as a function of poststretching dwell time: (a) for material AF drawn at 120 °C and (b) for material R drawn at 105 °C. Drawing was performed at a strain rate 0.02 s^{-1}, to a draw ratio $\lambda = 3$, and was followed by relaxation at the test temperature for a specified dwell time prior to quenching. Also shown are simulation predictions of birefringence using models with (solid lines) and without (dashed lines) finite extensibility. Also illustrated are the dwell times at which the τ_e- and τ_R-based Deborah numbers are equal to unity.

prior to freezing, and Figure 6b for material R drawn to $\lambda = 3$ at 105 °C and relaxed for t_{dwell} prior to freezing. Both materials were drawn at a nominal strain rate of 0.02 s^{-1}.

The monodisperse material AF was stretched at a rate where $Wi_e < 1$, and relaxation of the birefringence can be observed to start at $De_e \approx 1$. The birefringence continues to drop further even for $De_R^{AF} < 1$. The polydisperse material R was stretched at a rate where $Wi_e > 1$, and relaxation of the birefringence is evident even at short dwell times where $De_e > 1$.

Also shown in Figure 6a,b are simulations of birefringence computed using the constitutive model. In the monodisperse material AF, the hot drawing was performed at $Wi_e < 1$, and hence no subentanglement stretch is applied during stretching. The model with FE (solid line) predicts the birefringence remarkably accurately for all the different values of dwell time investigated. The model without FE overpredicts the birefringence for all conditions. The polydisperse material R was hot-drawn at $Wi_e > 1$, and therefore shortcomings in model predictions are to be expected since the material will experience subentanglement stretch during hot drawing. In fact, in this case the model performs poorly throughout the
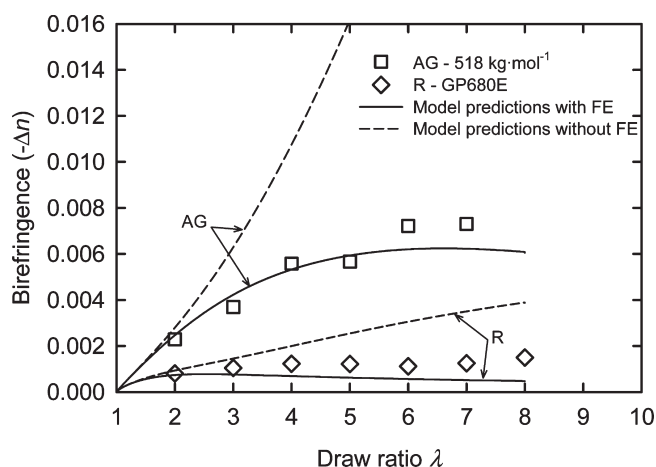
predictions. For the same reasons explained previously in the role of temperature, the use of the Rolie−Poly model in its present form appears to be inappropriate for capturing the dwell-time relaxation in *polydisperse* materials drawn under these conditions.

The Role of Draw Ratio. Figure 7 shows measurements of birefringence as a function of draw ratio λ, for materials AG and R drawn at 135 °C and immediately quenched. Materials were drawn at a nominal strain rate of 0.02 s^{-1} to a stretch λ varying from 2 to 8. In this case, for both materials, the stretching occurs at a rate where $Wi_e < 1 < Wi_R$. The birefringence rises initially with draw ratio up to $\lambda \approx 4$ and then levels off to an approximately constant value at higher draw ratios.

Also shown in Figure 7 are computed simulations of birefringence from the constitutive model. In the monodisperse material AG, use of the model with FE (solid line) produces accurate predictions of birefringence across the full range of draw ratios. Removing finite chain extensibility results in no saturation of birefringence with chain stretch, and the model (dashed line) significantly overpredicts the birefringence for large stretches in the monodisperse material. For the polydisperse material, the model with FE underpredicts birefringence and the model without FE overpredicts birefringence. This is consistent with previous observations.

In summary, the methodology employing the constitutive model presented is appropriate for accurate predictions of locked-in birefringence in oriented monodisperse materials, provided that there is no significant chain stretch at the subentanglement level. In most contexts this equates to $Wi_e < 1$. Typical polymer processing operations such as extrusion and injection molding do not normally introduce significant amounts of subentanglement level chain stretch, and thus the model is promising in this context. In its present form, the model is less successful for predictions of birefringence in polydisperse materials. The different procedures have also illustrated the need for finite chain extensibility in achieving quantitatively accurate birefringence predictions.

■ CONCLUSIONS

This work has presented a methodology for the use of a recently proposed molecularly aware constitutive model for polymer glasses[8] in making predictions of birefringence in oriented glassy polymers

and has validated its predictions. The constitutive model consists of a coupling of the Likhtman−Graham Rolie−Poly melt rheology model, allowing for finite extensibility, and a previously established model for polymer glasses. Experimental validation was performed through a series of experiments designed to produce frozen-in molecular orientation in samples of monodisperse and polydisperse PS. Although the two parts of the model contribute independently to birefringence, only the conformational part was significant in the experimental validation. The variables investigated were draw temperature, stretch ratio, and dwell time before quenching through T_g. The constitutive model was able to quantitatively predict birefringence in monodisperse PS for orientation processes sufficiently far above T_g (i.e., not including subentanglement stretch). Accurate quantitative predictions were not possible for polydisperse PS.

Although the methodology presented here should be especially useful in optimizing the optical properties of polymer products, by reducing the need for prior characterization and experimentation, an extension to typical commercial polydisperse polymers will require the development of a nonlinear rheological model that accounts for polydispersity.

■ APPENDIX. ROLIE−POLY WITH FINITE EXTENSIBILITY

A typical molecule at some instant has end-to-end vector $\mathbf{R}$, while in the relaxed state at the origin of time this was $\mathbf{R}_0$. The orientation tensor $\mathbf{T}$ and an rms average molecular stretch λ are defined as follows in terms of the ensemble averages of these two vectors:

$$\mathbf{T} \equiv 3\frac{\langle \mathbf{R}\mathbf{R}^T \rangle}{\langle R_0^2 \rangle}; \quad \lambda \equiv \frac{\langle R^2 \rangle^{1/2}}{\langle R_0^2 \rangle^{1/2}} = \sqrt{\frac{\text{tr } \mathbf{T}}{3}} \qquad (A.1)$$

The general form of the Rolie−Poly model (in the absence of convective constraint release) is (see ref 10)

$$\dot{\mathbf{T}} = \overline{\mathbf{L}}\cdot\mathbf{T} + \mathbf{T}\cdot\overline{\mathbf{L}}^T - \frac{1}{\tau_d}(\mathbf{T} - \lambda^2 \mathbf{I}) - f_{\text{retr}}(\text{tr } \mathbf{T})\mathbf{T} \qquad (A.2)$$

Suppose the polymer melt is stress-relaxing in the absence of any velocity gradient, and we consider a time scale very short compared to the reptation time, then the rate of relaxation of molecular stretch by retraction within the tube is obtained by taking the trace of eq A.2 and may be represented as follows:

$$\frac{d\lambda}{dt} = -f_{\text{retr}}(\lambda)\frac{\lambda}{2} \qquad (A.3)$$

If we consider the molecular stretch and viscous flow within the tube as behaving like a spring and dashpot in series, with an effective viscosity μ, and the end-to-end entropic force f as that of a Gaussian chain extended to the rms average stretch, the rate of relaxation will be given by

$$\mu\frac{d\lambda}{dt} = -f = -\frac{3kT}{\langle R_0^2 \rangle^{1/2}}(\lambda - 1) \qquad (A.4)$$

Comparing this to the general equation for the rate of relaxation of a linear spring−dashpot system yields an expression for the time constant for retraction within the tube:

$$\frac{d\lambda}{dt} = -\frac{(\lambda - 1)}{\tau_R}; \quad \text{hence } \tau_R = \frac{\mu\langle R_0^2 \rangle^{1/2}}{3kT} \qquad (A.5)$$

Repeating these steps, but invoking instead the end-to-end entropic force f of a freely orienting chain with a finite number n of links with length l and extended to the rms average stretch, eq A.4 is replaced by

$$\mu\frac{d\lambda}{dt} = -f$$

$$= -\frac{3kT}{\langle R_0^2 \rangle^{1/2}}\left[\frac{\langle R_0^2 \rangle^{1/2}}{3l}\mathscr{L}^{-1}\left(\frac{\langle R^2 \rangle^{1/2}}{nl}\right) - 1\right] \qquad (A.6)$$

where $\mathscr{L}^{-1}(x)$ is the inverse Langevin function. It follows from eq A.3 that, in this case of finite molecular extensibility, the Rolie−Poly term f_{retr} takes the form

$$f_{\text{retr}} = \frac{2}{\tau_R}\left(\frac{\frac{\lambda_{\max}}{3}\mathscr{L}^{-1}\left(\frac{\lambda}{\lambda_{\max}}\right) - 1}{\lambda}\right) \qquad (A.7)$$

where the limiting stretch is $\lambda_{\max} = \sqrt{n}$. Although eq A.7 is what results if the force f is assigned precisely the value for an inverse-Langevin chain, there is a small but important inaccuracy in eq A.7, since it does not satisfy the physical requirement $f_{\text{retr}} \rightarrow 0$ as $\lambda \rightarrow 1$. Consequently, for consistency, it is necessary to divide the first term in the numerator bracket of eq A.7 by its value at $\lambda = 1$: a correction factor close to unity. We employ the Padé approximation to $\mathscr{L}^{-1}(1/\lambda_{\max})$ and hence obtain (see eqs 12 and 13)

$$f_{\text{retr}} = \frac{2}{\tau_R}\left(\frac{F(\lambda) - 1}{\lambda}\right), \quad \text{where } F \equiv \frac{\mathscr{L}^{-1}(\lambda/\lambda_{\max})}{\mathscr{L}^{-1}(1/\lambda_{\max})}$$

$$= \frac{\lambda_{\max}}{3}\left[\frac{\lambda_{\max}^2 - 1}{\lambda_{\max}^2 - 1/3}\right]\mathscr{L}^{-1}\left(\frac{\lambda}{\lambda_{\max}}\right) \qquad (A.8)$$

Consider now the conformational stress generated by molecular alignment. The retractive force vector on a particular chain, allowing for finite extensibility, is well-known:

$$f = \frac{kT}{l}\mathscr{L}^{-1}\left(\frac{R}{nl}\right)\frac{\mathbf{R}}{R} \qquad (A.9)$$

If there are N such chains per unit initial volume, the effective cross-section area perpendicular to $\mathbf{R}$ in the stretched state is $(NR/J)^{-1}$, and the conformational stress contributed by chains with end-to-end vector $\mathbf{R}$ would then be

$$\boldsymbol{\sigma}_{c, \mathbf{R}} = \frac{NkT}{Jl}\mathscr{L}^{-1}\left(\frac{R}{nl}\right)\frac{\mathbf{R}\mathbf{R}^T}{R} \qquad (A.10)$$

while the stress from an ensemble of chains with many different $\mathbf{R}$ would be

$$\boldsymbol{\sigma}_c = \frac{NkT}{Jl}\left\langle \mathscr{L}^{-1}\left(\frac{R}{nl}\right)\frac{\mathbf{R}\mathbf{R}^T}{R}\right\rangle \qquad (A.11)$$

There is no analytical solution for the average appearing in eq A.11. Therefore, consistent with eq A.6, we take R to refer to a chain with the rms average stretch and approximate eq A.11 by

$$\boldsymbol{\sigma}_{\rm c} = \frac{1}{J}\frac{NkT}{nl^2}\frac{nl}{\langle R^2\rangle^{1/2}}\mathscr{L}^{-1}\left(\frac{\langle R^2\rangle^{1/2}}{nl}\right)\langle \mathbf{RR}^{\rm T}\rangle$$

$$= \frac{NkT}{J}\frac{\lambda_{\max}}{3\lambda}\mathscr{L}^{-1}\left(\frac{\lambda}{\lambda_{\max}}\right)\mathbf{T} \qquad (A.12)$$

As in the derivation of eq A.7 using a similar approximation, eq A.12 contains a small inconsistency with the non-FE calculation of the "entanglement" shear modulus from Gaussian statistics applied to the portions of chains contained within one tube diameter $G_{\rm e} = NkT$. Employing the function F from eq A.8 corrects for this, giving the result[45]

$$\boldsymbol{\sigma}_{\rm c} = \frac{G_{\rm e}}{J}\frac{F(\lambda)}{\lambda}\mathbf{T} - p\mathbf{I} \qquad (A.13)$$

where we also acknowledge that stress $\boldsymbol{\sigma}_{\rm c}$ in eq A.12 is known only to within a hydrostatic back-stress here labeled p. This is eliminated in calculating the deviatoric conformational stress thus (see eq 11)

$$\mathbf{S}_{\rm c} = \boldsymbol{\sigma}_{\rm c} - \frac{1}{3}\,{\rm tr}\,\boldsymbol{\sigma}_{\rm c}\,\mathbf{I} = \frac{G_{\rm e}}{J}\frac{F(\lambda)}{\lambda}[\mathbf{T} - \lambda^2\mathbf{I}] \qquad (A.14)$$

Finally, it is interesting to note that the tensor $\mathbf{T}$ employed here, defined precisely in molecular terms in eq A.1, provides a physical interpretation for the "elastic" or "network" left Cauchy−Green tensor that appears in more empirical treatments of amorphous polymer viscoelasticity. Thus, if $\mathbf{F}^{\rm n}$ refers to the deformation gradient inflicted on the molecular end-to-end vectors, each initial $\mathbf{R}_0$ transforms to $\mathbf{R} = \mathbf{F}^{\rm n}\mathbf{R}_0$, and the initially isotropic distribution of $\mathbf{R}_0$ vectors imposes

$$\langle \mathbf{R}_0\mathbf{R}_0^{\rm T}\rangle = \frac{1}{3}\langle R_0{}^2\rangle\mathbf{I}, \quad \text{hence } \mathbf{T} \equiv 3\frac{\langle \mathbf{RR}^{\rm T}\rangle}{\langle R_0{}^2\rangle}$$

$$= 3\frac{\langle \mathbf{F}^{\rm n}\mathbf{R}_0\mathbf{R}_0^{\rm T}\mathbf{F}^{\rm nT}\rangle}{\langle R_0{}^2\rangle} = \mathbf{F}^{\rm n}\mathbf{F}^{\rm nT} = \mathbf{B}^{\rm n} \qquad (A.15)$$

Substituting $\mathbf{B}^{\rm n}$ for $\mathbf{T}$ in eq A.14 reveals that this expression for the deviatoric stress is essentially the same as that derived from the semiempirical "8-chain" model of Boyce and co-workers (see for example ref 29) although the latter lacks the correction term (square bracketed) in eq A.8 and therefore suffers from a small inconsistency with the Gaussian chain limit when $\lambda \to 1$.

■ AUTHOR INFORMATION

Corresponding Author
*Tel +44 115 9514097; Fax + 44 115 9514115; e-mail davide.defocatiis@nottingham.ac.uk.

Present Addresses
[†]Department of Chemical and Environmental Engineering, University of Nottingham, Nottingham NG7 2RD, UK.

■ ACKNOWLEDGMENT

■ REFERENCES

(1) Stein, R. S.; Finkelstein, R. S. *Annu. Rev. Phys. Chem.* **1973**, *24*, 207–234.

(2) Janeschitz-Kriegl, H. Polymer melt rheology and flow birefringence. In *Polymers, Properties and Applications*; Springer-Verlag: Berlin, 1983; Vol. 6.

(3) Tadmor, Z. *J. Appl. Polym. Sci.* **1974**, *18* (6), 1753–1772.

(4) Isayev, A. I.; Hieber, C. A. *Rheol. Acta* **1980**, *19* (2), 168–182.

(5) Isayev, A. I. *Polym. Eng. Sci.* **1983**, *23* (5), 271–284.

(6) Flaman, A. A. M. *Polym. Eng. Sci.* **1993**, *33* (4), 193–201.

(7) Flaman, A. A. M. *Polym. Eng. Sci.* **1993**, *33* (4), 202–210.

(8) De Focatiis, D. S. A.; Embery, J.; Buckley, C. P. *J. Polym. Sci., Part B: Polym. Phys.* **2010**, *48* (13), 1449–1463.

(9) Buckley, C. P.; Jones, D. C. *Polymer* **1995**, *36* (17), 3301–3312.

(10) Likhtman, A. E.; Graham, R. S. *J. Non-Newtonian Fluid Mech.* **2003**, *114*, 1–12.

(11) Graham, R. S.; Likhtman, A. E.; McLeish, T. C. B. *J. Rheol.* **2003**, *47* (5), 1171–1200.

(12) Wu, J. J.; Buckley, C. P. *J. Polym. Sci., Part B: Polym. Phys.* **2004**, *42* (11), 2027–2040.

(13) Dooling, P. J.; Buckley, C. P.; Rostami, S.; Zahlan, N. *Polymer* **2002**, *43* (8), 2451–2465.

(14) Bishko, G. B.; Harlen, O. G.; McLeish, T. C. B.; Nicholson, T. M. *J. Non-Newtonian Fluid Mech.* **1999**, *82* (2−3), 255–273.

(15) Lee, K; Mackley, M. R.; McLeish, T. C. B.; Nicholson, T. M.; Harlen, O. G. *J. Rheol.* **2001**, *45* (6), 1261–1277.

(16) Bent, J.; Hutchings, L. R.; Richards, R. W.; Gough, T.; Spares, R.; Coates, P. D.; Grillo, I.; Harlen, O. G.; Read, D. J.; Graham, R. S.; Likhtman, A. E.; Groves, D. J.; Nicholson, T. M.; McLeish, T. C. B. *Science* **2003**, *301*, 2691–1695.

(17) Collis, M. W.; Lele, A. K.; Mackley, M. R.; Graham, R. S.; Groves, D. J.; Likhtman, A. E.; Nicholson, T. M.; Harlen, O. G.; McLeish, T. C. B.; Hutchings, L. R.; Fernyhough, C. M.; Young, R. N. *J. Rheol.* **2005**, *49* (2), 501–522.

(18) Likhtman, A. E.; McLeish, T. C. B. *Macromolecules* **2002**, *35*, 6332–6343.

(19) De Focatiis, D. S. A.; Buckley, C. P. *Polym. Test.* **2008**, *27* (2), 136–145.

(20) De Focatiis, D. S. A.; Buckley, C. P.; Hutchings, L. R. *Macromolecules* **2008**, *41*, 4484–4491.

(21) Haward, R. N.; Thackray, G. *Proc. R. Soc. London, Ser. A* **1968**, *302*, 453–472.

(22) Govaert, L. E. *J. Polym. Sci., Part B: Polym. Phys.* **2004**, *42*, iii–iv.

(23) Buckley, C. P.; Dooling, P. J.; Harding, J.; Ruiz, C. *J. Mech. Phys. Solids* **2004**, *52* (10), 2355–2377.

(24) Boyce, M. C.; Parks, D. M.; Argon, A. S. *Mech. Mater.* **1988**, *7* (1), 15–33.

(25) Tervoort, T. A.; Smit, R. J. M.; Brekelmans, W. A. M.; Govaert, L. E. *Mech. Time-Depend. Mater.* **1998**, *1*, 269–291.

(26) Arruda, E. M.; Boyce, M. C.; Jayachandran, R. *Mech. Mater.* **1995**, *19* (2−3), 193–212.

(27) Meijer, H. E. H.; Govaert, L. E. *Prog. Polym. Sci.* **2005**, *30* (8−9), 915–938.

(28) Bardenhagen, S. G.; Stout, M. G.; Gray, G. T. *Mech. Mater.* **1997**, *25* (4), 235–253.

(29) Boyce, M. C.; Socrate, S.; Llana, P. G. *Polymer* **2000**, *41* (6), 2183–2201.

(30) Nagasawa, M.; Koizuka, A.; Matsuura, K.; Horita, M. *Macromolecules* **1990**, *23* (24), 5079–5082.

(31) Rudd, J. F.; Andrews, R. D. *J. Appl. Phys.* **1960**, *31* (5), 818–826.

(32) Luap, C.; Karlina, M.; Schweizer, T.; Venerus, D. C. *J. Non-Newtonian Fluid Mech.* **2006**, *138* (2−3), 197–203.

(33) van Krevelen, D. W. *Properties of Polymers: Their Correlation with Chemical Structure, Their Numerical Estimation and Prediction from Additive Group Contributions*, 3rd ed.; Elsevier: Amsterdam, 1990.

(34) Shimo, T.; Nagasawa, M. *Macromolecules* **1992**, *25* (19), 5026–5029.

(35) Ramirez, J.; Likhtman, A. E. Rheology of Entangled Polymers: Toolbox for the Analysis of Theory and Experiments (Reptate). http://www.reptate.com.

(36) Ward, I. M. *Structure and Properties of Oriented Polymers*; Applied Science Publishers Ltd.: Cambridge, 1975.

(37) Muller, R.; Pesce, J. J. *Polymer* **1994**, *35* (4), 734–739.

(38) Inoue, T.; Ryu, D. S.; Osaki, K. *Macromolecules* **1998**, *31* (20), 6977–6983.

(39) Kuhn, W.; Grün, F. *Kolloid Z.* **1942**, *101* (3), 248–271.

(40) Treloar, L. R. G. *Trans. Faraday Soc.* **1947**, *43* (5), 277–284.

(41) Arruda, E. M.; Boyce, M. C.; Jayachandran, R. *Mech. Mater.* **1995**, *19* (2−3), 193–212.

(42) Treloar, L. R. G. *Trans. Faraday Soc.* **1954**, *50*, 881–896.

(43) Matsumoto, T.; Bogue, D. C. *J. Polym. Sci., Part B: Polym. Phys.* **1977**, *15* (9), 1663–1674.

(44) Takahashi, S.; Saito, H. *Macromolecules* **2004**, *37* (3), 1062–1066.

(45) Note that in our previous application of the model (see ref 8) we approximated $J = 1$ when computing $\mathbf{S}^c$, on the grounds that its deviation from unity is negligible in comparison to experimental uncertainty in measured stresses. We include it here for completeness.